European Journal of Radiology 120 (2019) 108692

Contents lists available at ScienceDirect

European Journal of Radiology

journal homepage: www.elsevier.com/locate/ejrad

Research article

Deep learning-enabled system for rapid pneumothorax screening on chest CT*

Xiang Li*, James H. Thrall, Subba R. Digumarthy, Mannudeep K. Kalra, Pari V. Pandharipande, Bowen Zhang, Chayanin Nitiwarangkul, Ramandeep Singh, Ruhani Doda Khera, Quanzheng Li

Massachusetts General Hospital, Department of Radiolgoy, United States

ARTICLE INFO

Keywords:
Chest CT
Pneumothorax
Deep learning

ABSTRACT

Purpose: Prompt diagnosis and quantitation of pneumothorax impact decisions pertaining to patient management. The purpose of our study was to develop and evaluate the accuracy of a deep learning (DL)-based image classification program for detection of pneumothorax on chest CT.

Method: In an IRB approved study, an eight-layer convolutional neural network (CNN) using constant-size (36*36 pixels) 2D image patches was trained on a set of 80 chest CTs, with (n = 50) and without (n = 30) pneumothorax. Image patches were classified based on their probability of representing pneumothorax with subsequent generation of 3D heat-maps. The heat maps were further defined to include 1) pneumothorax area size, 2) relative location of the region to the lung boundary, and 3) a shape descriptor based on regional anisotropy. A support vector machine (SVM) was trained for classification.

Result: We assessed performance of our program in a separate test dataset of 200 chest CT examinations, with (160/200, 75%) and without (40/200, 25%) pneumothorax. Data were analyzed to determine the accuracy, sensitivity, specificity. The subject-wise sensitivity was 100% (all 160/160 pneumothoraces detected) and specificity was 82.5% (33 true negative/40). False positive classifications were primarily related to emphysema and/or artifacts in the test images.

Conclusion: This deep learning-based program demonstrated high accuracy for automatic detection of pneumothorax on chest CTs. By implementing it on a high-performance computing platform and integrating the domain knowledge of radiologists into the analytics framework, our method can be used to rapidly pre-screen large numbers of cases for presence of pneumothorax, a critical finding.

1. Introduction

Pneumothorax is a potentially life-threatening condition characterized by the abnormal presence of free air in the pleural space [1–3]. Pneumothorax is a critical finding, that often requires emergent communication of the imaging results and intervention [4–6]. Computed Tomography (CT) imaging of the chest and its quantative analysis has been shown to be promising for lung disease diagnosis and prognosis [7–9]. However, timely interpretation can be challenging when chest CT examinations cannot be reviewed immediately as may occur periodically when queues of cases waiting for interpretation accrue. Moreover, not all imaging departments have on-site coverage by radiologists 24 h a day. A rapid system for detecting pneumothorax on chest CTs, run automatically upon their completion, could be used to send alerts to radiologists and other healthcare providers, to reprioritize the chest CT work list for cases with pneumothoraces.

Deep learning (DL) programs based on convolutional neural networks (CNN) have achieved very high performance for computer vision tasks in natural image processing such as facial recognition [10], as well as in medical image analysis including CT and PET image reconstruction [11,12] and skin cancer diagnosis [13]. The dense structure of CNNs with learned image filers (i.e. convolutional layers) and classifiers (i.e. deep fully-connected layers) offers better data representation and generalizability than most traditional machine learning approaches [14]. This improves robustness of performance in real-world applications [15]. These advances in deep learning-based image analysis have spurred research in radiology, such as segmentation, detection and diagnosis/prognosis in cardiovascular imaging [16], detection and characterization of lung nodules [17], detection of pulmonary tuberculosis [18] and detection of mass effects, hydrocephalus

* This work is originated from Massachusetts General Hospital, Department of Radiology, 55 Fruit St, Boston, MA 02114

* Corresponding author at: 25 New Chardon St. 449A, Boston, MA, 02114, United States.
E-mail address: xli60@mgh.harvard.edu (X. Li).

https://doi.org/10.1016/j.ejrad.2019.108692
Received 19 April 2019; Received in revised form 13 September 2019; Accepted 19 September 2019

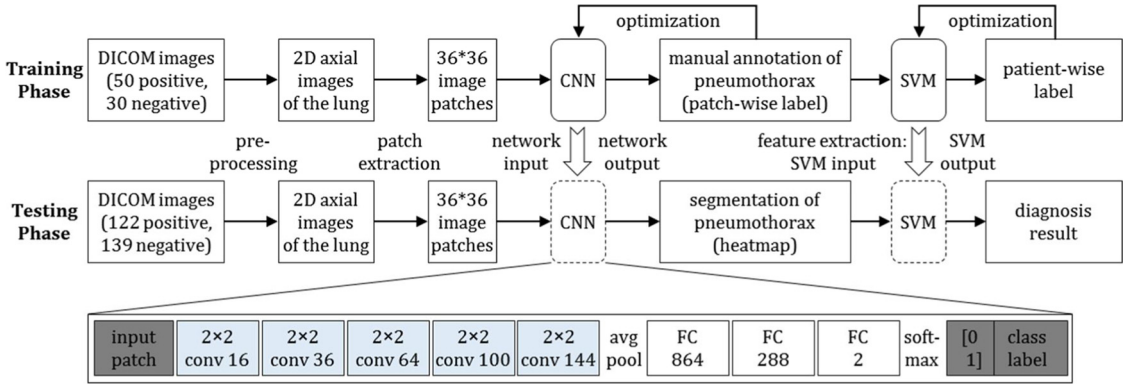

Fig. 1. The algorithmic pipeline of the system, showing the data flow from DICOM inputs to the diagnostic result within the training and testing phases.

and hemorrhage in the brain [19].

The purpose of our study was to develop a rapid deep learning (DL)-based image analysis program for automatic detection of pneumothoraces on chest CT.

2. Materials and methods

This study was approved by the institutional review board. The study was compliant with the Human Insurance Portability and Accountability Act (HIPAA).

The algorithmic pipeline is illustrated in Fig. 1. The work consisted of a training and a testing phase: within the training phase, a deep convolutional neural network was trained and validated based on CT images with their corresponding annotations of pneumothorax. Regional features of pneumothorax including lesion size, relative location, and shape were extracted from the regions with pneumothorax, and used to train a Support Vector Machine (SVM) to map pneumothorax image features with the patient-wise label (with/without pneumothorax). Within the testing phase, labels of input patches predicted by the network were combined to segment the region with pneumothorax (i.e. heatmap). The SVM utilized these heatmaps to generate patient-wise diagnoses of pneumothorax. Inputs to the proposed program are DICOM images of chest CTs, and outputs of the proposed program are patient-wise predicted labels (with/without pneumothorax), thus achieving an end-to-end framework for pneumothorax screening.

2.1. Patients

We identified chest CT cases of 280 patients with age range 2–115 years (mean 56.04 ± 22.81), of 194 males and 86 females, including 210 with pneumothorax (positive) and 70 without pneumothorax (negative), using a free text search in a radiology report repository with keywords ("pneumothorax" and "chest CT") and subsequent consensus of two expert thoracic radiologists. Mean values of CT dose index ($CTDI_{VOL}$) and Dose Length Product (DLP) for the 280 CT scans were 7.3 mGy and 239.1 mGy·cm, respectively. Identified cases were randomly assigned to either training (n = 76, 46 with pneumothorax, 30 without pneumothorax), validation (4, all with pneumothorax) or testing (n = 200, 160 with pneumothorax, 40 without pneumothorax) datasets.

2.2. CT image data and preprocessing

All chest CT scans were performed with routine chest CT protocols for clinically indicated reasons. The CT examinations were performed on one of the 18 CT scanners in our hospital (ranging from 16- to 128-detector row multidetector CT). The scanners belonged to three different CT vendors (GE, Siemens and Philips).

We exported transverse DICOM image series reconstructed with 2.5–3 mm section thickness and standard reconstruction techniques (commercial filtered back projection or iterative reconstruction, based on scanner type). The exported DICOM images were preprocessed to lung window settings [−500, 1400], with lung segmentation and normalization using well-established unsupervised algorithms. Additional details of the lobe and main trachea segmentation are included in the Appendix and have been described previously in [20].

2.3. Annotation and diagnostic standard

Manual annotation of regions with pneumothorax was performed on an image-by-image basis in the transverse CT images of each patient in the learning set. The annotation was represented as a 3D binary mask indicating the presence of pneumothorax on each voxel, i.e. positive, with label of "1" or negative, with label of "0". Uniform image patches of 36 × 36 pixels extracted from the lung regions were used as CNN input with a stride of 4 (i.e. distance between the center of two neighboring patches is 4 pixels in any direction). The label of each patch was determined based on the annotation label of its center voxel. See Appendix for additional discussion of image patches.

Manual image annotation in the training set was performed by research fellows under the supervision of three radiologists (JHT with 40 years of experience, SRD with 22 years of experience, and MKK with 19 years of experience).

2.4. CNN architecture and classification model for diagnosis: training phase

In this project, an eight-layer Convolutional Neural Network (CNN) was trained. The architecture of the network is shown in the bottom panel of Fig. 1, where we used five stacked 2 × 2 convolutional kernels with pooling for image feature representation and three fully connected networks for patch classification. This network structure has been applied for classification and diagnosis of interstitial lung diseases (micronodules, reticulation, etc.) and achieved superior performance [21]. The system is implemented in the Caffe Deep Learning Framework in the Python programming language, and deployed on a NVIDIA DGX station equipped with 8 T P100 GPUs (NVIDIA Inc). Input of the network is constant-sized (36 × 36) 2D image patches extracted from the training set. In this work, we adopted 2D image analysis rather than 3D because slice thickness (i.e. z-axis resolution) varied across patients due to different scanner settings.

The teaching output of the network is the manually-annotated labels of the corresponding patches. The training was performed to minimize the error between the true labels of the patches and the predicted labels from the network, where the residual was back propagated to update the parameters of each layer in the network. The training process consisted of 25 total passes through the whole training dataset for backpropagation optimization (i.e. epoch = 25), where the epoch

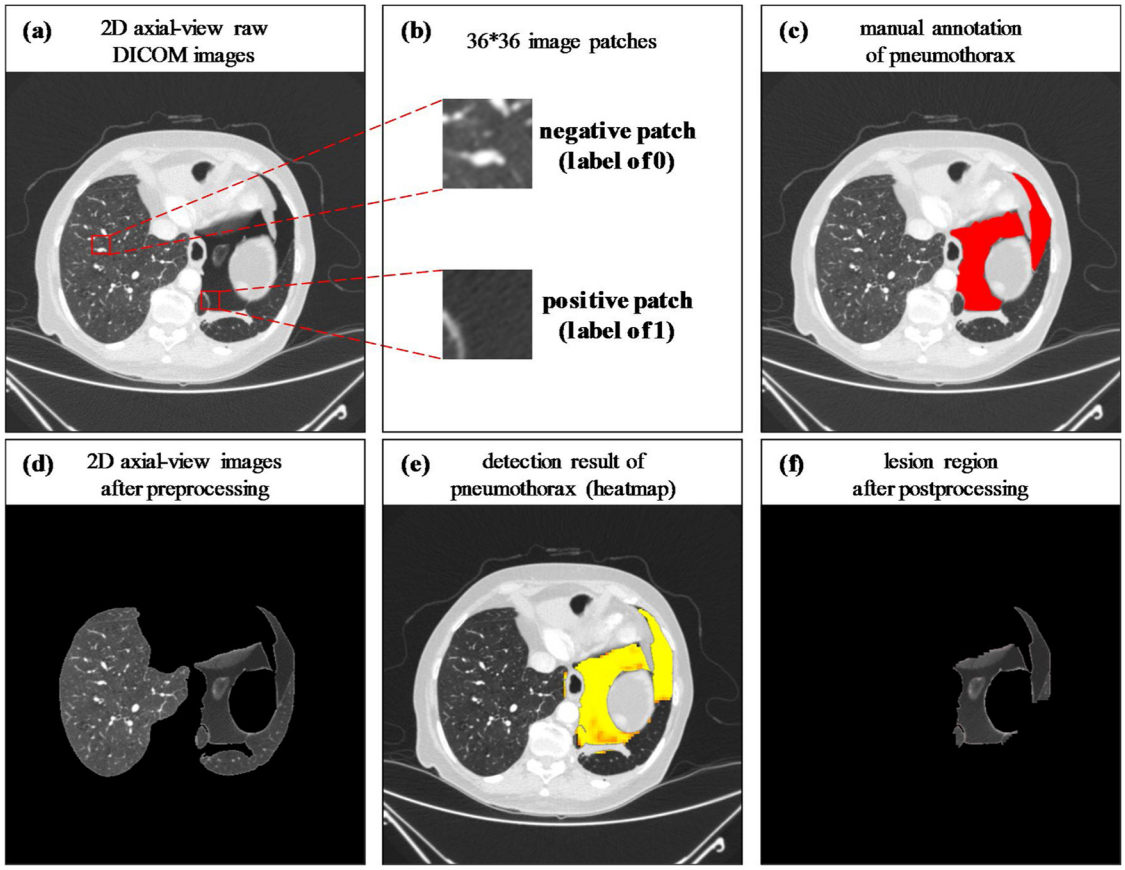

Fig. 2. Running example of a pneumothorax lesion region detection process output at various intermediate steps within the system; starting with a single transverse image (a), image patches extraction (b), annotated image (c), lung segmentation (d), heat map (e) and segmentation of the pneumothorax (f).

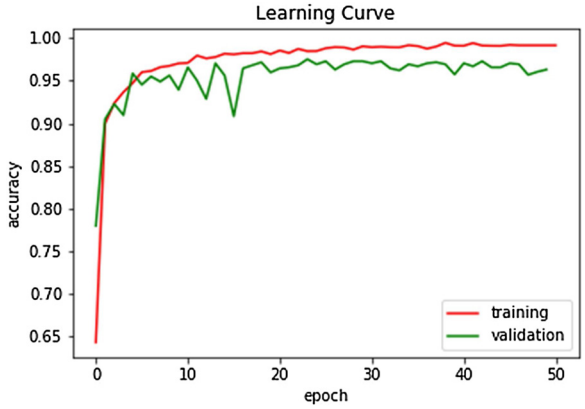

Fig. 3. Learning curve of the CNN model along the training process. x-axis: epoch number (training progress), y-axis: training/validation loss of the network.

number was determined according to training loss and validation loss with early stopping, as shown in Fig. 3. We used Adam optimizer for optimization with exponential decay learning rate (initial learning rate = 10^{-3}, weight decay = 10^{-8}). After each training epoch, the network performance was evaluated on the validation dataset. In addition to training the CNN, we also trained an SVM from the image features of the annotation map as shown in Fig. 2c. Specifically, for each patient with pneumothorax, we extracted the following image features from the 3D annotation region: 1) relative size of the pneumothorax, that is, ratio between the size of pneumothorax and the size of the lung, 2) relative location of the pneumothorax, measured by the distance between the centroid of the pneumothorax region to the nearest lung boundary, and 3) a shape descriptor based on regional anisotropy. The above image features were used as inputs for training the SVM with a Gaussian Radial Basis Function (RBF) kernel, where the training output of the SVM is the patient-wise label as either positive [1] or negative (0) for pneumothorax, as similarly performed in previous radiomics studies [22].

2.5. CNN architecture and SVM model for diagnosis: testing phase

After training the DL program, we assessed the performance on the test dataset with 80% (160/200) positive and 20% (40/200) negative cases. First, image patches extracted from each patient in the test set were classified based on probability of pneumothorax by the previously trained CNN. Patch-wise prediction results were then aggregated into a 3D heat-map for regions with pneumothorax. Afterwards, the heat-map was postprocessed by segmenting out the largest connected component based on the region growing algorithm, resulting in a single region of pneumothorax (Fig. 2e). Image features calculated from the post-processed result were then fed into the previously trained SVM, which performed the prediction (i.e. diagnosis) of whether a given patient had a pneumothorax or not [22].

2.6. Testing DL and human observer study

The SOR (standard of reference) of the 200-CT test set was provided by two thoracic subspecialty radiologists (SRD and MKK) through consensus evaluation for presence of pneumothorax (per patient true-positive cases of pneumothorax = 160, true-negative cases = 40). In addition, three radiologists (CN with 4 years of experience; RS with 2 years of experience; RDK with 1 year of experience) independently evaluated these 200 chest CT examinations without knowledge of DL or

SOR findings about pneumothorax, thus serving as test radiologists.

2.7. Statistical analysis

Differences in performance metrics (accuracy, sensitivity and specificity) between each test radiologist and the DL system, were evaluated using the Chi-Squared test. The generalized kappa (Fleiss' Kappa) statistic was also calculated to evaluate the interobserver agreement among the three radiologists. A significance level of $p < 0.05$ was used to determine whether the tests are statistically significant.

3. Results

SOR found unilateral pneumothorax in 138 chest CTs and bilateral pneumothoraces in 22 chest CTs; 40 chest CTs had no pneumothorax. Metallic hardware or image artifacts were noted in 11/200 chest CT examinations. Accuracies of the three test radiologists were 91.0%, 94.5%, 86.0% with respective sensitivities of 91.3%, 95.6%, 86.3%, and specificities of 90.0%, 90.0%, 85.0%. Sizes of pneumothorax ranged from small (few tens of voxels) to large (occupying the entire hemithorax). Locations of pneumothorax were variable and included apical, lateral, medial, and basilar distribution.

Overall patch-wise accuracy of the CNN was 94% (37,025,649/39,452,819 patches) for detecting the true label (with or without pneumothorax) of each patch, which effectively measures the overlapping areas between the predicted heat map and annotation. After the patch-wise results were aggregated, postprocessed and analyzed by the SVM model, the overall patient-wise accuracy for detection of pneumothorax was 96.5% (193/200 patients), which serves as the evaluation criterion for the system. The respective sensitivity and specificity were 100% (all 160/160 pneumothoraces detected) and 82.5% (33 true negative/40 patients without pneumothorax).

The DL program had 7 false positive classifications of pneumothorax in patients with large lung cysts or bullae (4 patients) and metal-related streak artifacts (3 patients). Two sample cases of false positive results from the model are in Fig. 4.

Using the Chi-Squared test, overall accuracy (96.5%) of the DL system was found significantly higher than the performance of two of the three human readers: (91% $p = 0.02$, 86% $p = 0.0002$). Sensitivity of the DL system was significantly higher than all three human readers: (91.3% $p = 0.0002$, 95.5% $p = 0.0007$ and 86.3% $p < 0.0001$). Specificity of the DL system is lower than all human observers, but was not significantly different (90% $p = 0.37$, 90% $p = 0.37$ and 85% $p = 0.76$). Fleiss' Kappa statistic shows that reliability for the three radiologists was found to be Kappa = 0.711 ($p < 0.0001$), which indicates that reader agreement is not due to chance.

Time cost for training (i.e. backpropagation algorithm for updating network parameters) the CNN on the patches extracted from the 80-subject training set was around 20 min, not including time cost for data preparation, preprocessing and postprocessing. The predicted in practice, average processing time for each CT examination on the NVIDIA DGX station was 151 s (< 3 min) with the following breakdown:

- DICOM files conversion to Python data: 23 s
- Preprocessing (windowing, segmentation and normalization): 82 s
- Patch extraction for preparing CNN input (about 2 million patches per patient): 30 s.
- CNN prediction on patches extracted: < 1 s.
- Postprocessing (heatmap generation from prediction results): 14 s
- Feature extraction from the heatmap and SVM classification: < 1 s

4. Discussion

To be effective for the stated purpose of surveilling just completed chest CTs for pneumothorax, an analytic program should run automatically, have high sensitivity and reasonable specificity and be fast enough to make a meaningful difference in prioritizing the work list. The high sensitivity of our automated DL enabled program coupled with the short processing time (< 3 min) meet these criteria.

Although small pneumothoraces may not be life threatening or require treatment, monitoring for stability or resolution is important as these can rapidly increase, and lead to catastrophic outcome. Such increase can happen spontaneously, or during air travel where air is subject to Boyle's law and can expand in volume as cabin pressure drops [23]. Hu et al have estimated that trapped air in the human body can expand by 25–30% at commercial airline cabin pressures that are typically equivalent to 8000 feet in altitude [20]. The current guidelines recommend delaying air travel for one to three weeks after thoracic surgery or resolution of a pneumothorax [20]. Per departmental policy, we try to notify attending physicians about all unexpected, new and increasing pneumothoraces as soon as possible, ideally while patients are still in the institution, so they can alert and advise their traveling patients before they have left the institution. Having a DL enabled surveillance program in place will help achieve this goal.

Although chest CT has been considered as the de facto "gold standard" or "ground truth" for the diagnosis of pneumothorax for more than three decades [24–28], to our best knowledge and literature review, there are no published reports on its accuracy for diagnosing pneumothorax or for assessing individual observer performance or interobserver variability. This underscores one of the overarching challenges for DL applications in medical imaging—the need for explicit descriptions of how ground truth was established [29]. In pneumothorax, release of free air at chest tube placement is more definitive than chest CT [25]. However, chest tube placement is reserved for patients with larger pneumothoraces, and is unnecessary for patients with smaller pneumothoraces. Thus, we used expert consensus as the standard of reference (SOR) in this work. It was also found that false positive pneumothorax diagnoses from human observation studies (test

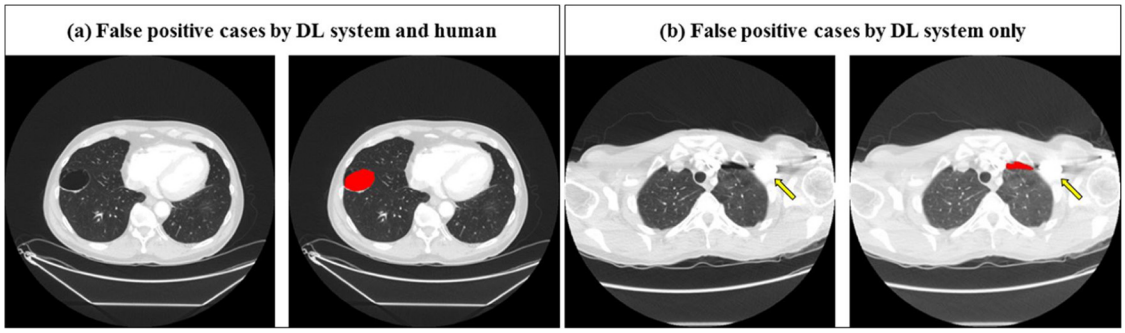

Fig. 4. False positive predictions of pneumothorax with the DL system. Segmentation results from the DL system for false positive pneumothoraces are highlighted in red. Apparent reasons for the false positives were (a) lung cyst, and (b) image artifact secondary to metallic implant (marked by yellow arrow) at the ventro-apical left area.

radiologists) are mainly due to presence of emphysema, image artifacts, and lung cystic fibrosis, conditions that can make it difficult to assess pneumothorax and result in artefactual appearance of pneumothorax.

Although there are no similar or historic studies with which to compare the entirety of our results, the work of Cai et al is partly comparable [30]. Cai et al described a non- DL approach to automated computer detection of pneumothoraces in selected trauma patients aimed also at measuring pneumothorax sizes. All included cases had an original radiologic diagnosis of pneumothorax. Seven of the 68 (10.3%) cases were determined by subsequent expert consensus review to not have pneumothoraces, i.e. were false positives on original interpretation.

The computer program developed by Cai et al [30] demonstrated a sensitivity of 100% for pneumothorax detection, the same as in our work, but had an overall false positive rate per case of 0.90 (area-wise), primarily due to the high prevalence of small false positive areas, limiting the usefulness of the approach for pneumothorax screening in unselected cases.

Cai et al applied an improved version of their program in pediatric patients [31]. Among 58 cases selected for having a proven pneumothorax, the program was 100% sensitive for detecting observer diagnosed pneumothoraces (63/63) but returned 5 additional areas (0.9% of cases) falsely determined to represent pneumothorax.

Although the method of case selection in Cai's studies [30,31] does not allow accuracy, sensitivity and specificity to be calculated for the original readers or compared directly to our results, the presence of false positives among the included cases for both human observers [30] and the computer program [30,31] is notable and at least qualitatively similar to the findings in our study.

In future years, as DL workflows evolve to prioritize multiple types of life-threatening findings on imaging studies, there will likely need to be further emphasis placed on specificity. The rationale for this delayed need is that in its infancy, DL workflows such as that described here will be used for a limited number of applications (e.g. pneumothorax, free intraperitoneal air, etc.), and on specialty or modality-specific worklists (e.g. chest x-rays). As such applications grow, if too many false-positive results occur – because of prioritizing sensitivity over specificity – less common life-threatening findings will be paradoxically de-prioritized. To avoid such a circumstance, as the number of successful AI algorithms grow, a data-driven, computational approach will be necessary to identify the optimal prioritization of each algorithm, considering the sensitivity and specificity of each algorithm, as well as the acuity and prevalence of the target finding.

There are limitations to our study. The study was retrospective with enriched numbers of positive cases. In an unselected prospective setting, the ratio of true positive cases versus all positive cases (positive predictive value) is likely to be quite different than in our learning and test sets. Therefore, it is important that interpreting radiologists understand the optimization strategy and are prepared to deal with false positives. This conundrum is likely to apply in many AI/DL applications where it is more practical to use enriched data sets for training and testing than unselected cases [16–18].

In our study, all patients came from a single institution. Even though we used separate training and test sets, there is still a possibility of "overfitting" the data due to the nature of our case mix. For example, given the false positives associated with lesions judged to be bullae, an institution with higher or lower percentages of patients with chronic lung disease might experience different results. This possibility can be addressed by testing the program in other institutional settings. Although processing time did not include image transfer time to our processing workstation, which can span several minutes, this limitation can be addressed with installation of DL programs directly on the CT scanners or the PACS.

Metallic implant related image artifacts are likely to represent a recurring challenge in imaging applications of DL. For example, Prevedello et al noted a false positive due to a metallic implant in their work on AI analysis of brain scans [18]. Wider availability of commercial metal artifact reduction algorithms, currently available on more advanced scanners, should substantially reduce artifacts related to metal implants and may decrease related errors in detection (17,32). These algorithms were not used in our study.

In conclusion, our highly sensitive DL enabled program enables rapid detection of pneumothorax on chest CT providing a DL-driven approach for optimization of clinical data management and processing. The program is not intended to be a stand-alone program to diagnose pneumothorax or replace the role of the radiologist. Rather, it is intended as a new tool to help radiologists optimize the flow of work for earlier detection of this important potentially life-threatening and often unsuspected finding. If successful, the clinical implementation of this program can serve as a model for other surveillance programs aimed at other potentially life-threatening diseases and conditions as well as programs aimed at segmenting cases into higher versus lower risk-of-disease categories more generally.

Funding

This work is supported by institutional funding from Massachusetts General Hospital.

Declaration of Competing Interest

There are no conflicts of interest from the authors for the submission of "Deep Learning-Enabled System for Rapid Pneumothorax Screening on Chest CT".

Appendix A. Supplementary data

Supplementary material related to this article can be found, in the online version, at doi:https://doi.org/10.1016/j.ejrad.2019.108692.

References

[1] S.A. Sahn, J.E. Heffner, Spontaneous pneumothorax, NEJM 342 (12) (2000) 868–874.
[2] J. Collins, E.J. Stern, Chest Radiology: The Essentials, third ed, LWW, 2014.
[3] M.H. Baumann, M. Noppen, Pneumothorax, Respirology 9 (2) (2004) 157–164.
[4] L. Yarmus, D. Feller-Kopman, Pneumothorax in the critically ill patient, CHEST 141 (4) (2019) 1098–1105.
[5] S. Hussain, Communicating critical test results in radiology, JACR 6 (2009) 148–151.
[6] H.B. Harvey, T.K. Alksab, P.V. Pandharipande, et al., Radiologist compliance with institutional guidelines for use of nonroutine communication of diagnostic results, JACR 12 (2015) 376–384.
[7] H. Kim, J.M. Goo, Y. Ohno, et al., Effect of reconstruction parameters on the quantitative analysis of chest computed tomography, J. Thorac. Imaging 34 (2) (2019) 92–102.
[8] M. Anthimopoulos, S. Christodoulidis, L. Ebner, A. Christe, S. Mougiakakou, Lung pattern classification for interstitial lung diseases using a deep convolutional neural network, IEEE Trans. Med. Imaging 35 (5) (2016) 1207–1216.
[9] S.J. Swensen, J.R. Jett, T.E. Hartman, et al., Lung cancer screening with ct: mayo clinic experience, Radiology (2003) 226.
[10] Y. Taigman, M. Yang, M. Ranzato, L. Wolf, DeepFace: closing the gap to human-level performance in face verification, IEEE Conference on Computer Vision and Pattern Recognition (2014) 1701–1708.
[11] D. Wu, K. Kim, G.E. Fakhri, Q. Li, Iterative low-dose CT reconstruction with priors trained by artificial neural network, IEEE Trans. Med. Imaging 36 (12) (2017) 2479–2486.
[12] K. Kim, D. Wu, K. Gong, et al., Penalized PET reconstruction using deep learning prior and local linear fitting, IEEE Trans. Med. Imaging 37 (6) (2018) 1478–1487.
[13] A. Esteva, B. Kuprel, R.A. Novoa, et al., Dermatologist-level classification of skin cancer with deep neural networks, Nature 542 (2017) 115–118.
[14] G.E. Hinton, R.R. Salakhutdinov, Reducing the dimensionality of data with neural networks, Science 313 (5786) (2006) 504–507.
[15] Y. LeCun, Y. Bengio, G. Hinton, Deep learning, Nature 521 (7553) (2015) 436–444.
[16] T. Retson, A.H. Besser, S. Sall, D. Golden, A. Hsiao, Machine learning and deep neural networks in thoracic and cardiovascular imaging, J. Thorac. Imaging 34 (3) (2019) 192–201.
[17] P. Lakhani, B. Sundaram, Deep learning at chest radiography: automated classification of pulmonary tuberculosis by using convolutional neural networks, Radiology 284 (2) (2017) 574–582.
[18] L.M. Prevedello, B.S. Erdal, J.L. Ryu, K.J. Little, M. Demirer, R.D. White, Automated

critical test findings identification and online notification system using artificial intelligence, Radiology 285 (2017) 923–931.
[19] B. Lassen, E.Mv Rikxoort, M. Schmidt, S. Kerkstra, Bv Ginneken, J.M. Kuhnigk, Automatic segmentation of the pulmonary lobes from chest CT scans based on fissures, vessels, and bronchi, IEEE Trans. Med. Imaging 32 (2) (2013) 210–222.
[20] M. Anthimopoulos, S. Christodoulidis, L. Ebner, A. Christe, S. Mougiakakou, Lung pattern classification for interstitial lung diseases using a deep convolutional neural network, IEEE Trans. Med. Imaging 35 (5) (2016) 1207–1216.
[21] R.T.H.M. Larue, G. Defraene, D. De Ruysscher, P. Lambin, W. van Elmpt, Quantitative radiomics studies for tissue characterization: a review of technology and methodological procedures, Br. J. Radiol. 90 (1070) (2016) 20160665.
[22] X. Hu, C.T. Cowl, M. Baqir, J.H. Ryu, Air travel and pneumothorax, CHEST 145 (2014) 688–694.
[23] S.D. Wall, M.P. Federle, R.B. Jeffrey, C.M. Brett, CT diagnosis of unsuspected pneumothorax after blunt abdominal trauma, AJR Am. J. Roentgenol. 141 (1983) 919–921.
[24] I.M. Tocino, M.H. Miller, P.R. Frederick, A.L. Bahr, F. Thomas, CT detection of occult pneumothorax in head trauma, AJR Am. J. Roentgenol. 143 (1984) 987–990.
[25] K. Alrajhi, My Woo, C. Vaillancourt, Test characteristics of ultrasonography for the detection of pneumothorax: a systematic review and meta-analysis, Chest 141 (2019) 703–708.
[26] K.R. Rowan, A.W. Kirkpatrick, D. Liu, K.E. Forkheim, J.R. Mayo, S. Nicolaou, Traumatic pneumothorax detection with thoracic US: correlation with chest radiography and CT—initial experience, Radiology 225 (1) (2002) 210–214.
[27] P. Kumari, Comparative analysis of efficacy of chest X-ray and chest CT scan in patients with chest trauma: a retrospective study, Int. J. Contemp. Med. Surg. Radiol. 2 (2017) 62–64.
[28] J.H. Thrall, X. Li, Q. Li, C. Cruz, S. Do, K. Dreyer, J. Brink, Artificial intelligence and depp learning in radiology: opportunities, challenges, pitfalls and criteria for success, JACR 15 (2018) 504–508.
[29] W. Cai, M. Tabbara, N. Takata, H. Yoshida, G.J. Harris, R.A. Novelline, M. Moya, MDCT for automated detection and measurement of pneumothoraces in trauma patients, AJR Am. J. Roentgenol. 192 (2009) 830–836.
[30] W. Cai, E.Y. Lee, Mahmood S.A. Vij, H. Yoshida, MDCT for computerized volumetry of pneumothoraces in pediatric patients, Acad. Radiol. 18 (2011) 315–323.
[31] N. Subhas, C.P. Pursyko, J.M. Polster, N.A. Obuchowski, F.F. Dong, et al., Dose reduction with didicated metal artifact reduction algorithm: CT phantom study, AJR 210 (2018) 593–600.